Journal of Solid State Chemistry 237 (2016) 36–47

Contents lists available at ScienceDirect

Journal of Solid State Chemistry

journal homepage: www.elsevier.com/locate/jssc

# Periodic density functional theory study of structural and electronic properties of single-walled zinc oxide and carbon nanotubes

Naiara L. Marana [a], Anderson R. Albuquerque [b], Felipe A. La Porta [c], Elson Longo [d], Julio R. Sambrano [a,*]

[a] Modeling and Molecular Simulations Group, São Paulo State University, UNESP, 17033-360 Bauru, SP, Brazil
[b] Federal Institute of Education, Science and Technology of Sertão Pernambucano, 56400-000 Floresta, PE, Brazil
[c] Chemistry Department, Federal Technological University of Paraná, 86036-370 Londrina, PR, Brazil
[d] São Paulo State University, Chemistry Institute, UNESP, 14801-907 Araraquara, SP, Brazil

ARTICLE INFO

*Article history:*
Received 23 November 2015
Received in revised form
20 January 2016
Accepted 22 January 2016
Available online 22 January 2016

*Keywords:*
ZnO nanotubes
DFT
Strain energy

ABSTRACT

Periodic density functional theory calculations with the B3LYP hybrid functional and all-electron Gaussian basis set were performed to simulate the structural and electronic properties as well as the strain and formation energies of single-walled ZnO nanotubes (SWZnONTs) and Carbon nanotubes (SWCNTs) with different chiralities as functions of their diameters. For all SWZnONTs, the band gap, strain energy, and formation energy converge to ~4.5 eV, 0.0 eV/atom, and 0.40 eV/atom, respectively. This result suggests that the nanotubes are formed more easily from the surface than from the bulk. For SWCNTs, the strain energy is always positive, while the formation energy is negative for armchair and zigzag nanotubes, therefore suggesting that these types of nanotubes can be preferentially formed from the bulk. The electronic properties of SWCNTs depend on the chirality; all armchair nanotubes are metallic, while zigzag and chiral nanotubes can be metallic or semiconducting, depending on the *n* and *m* vectors.


## 1. Introduction

Single-walled carbon nanotubes (SWCNTs) [1–5] have attracted great scientific and technological interest in nanoscience and nanotechnology fields, because of their unique chemical and physical properties.

In the last two decades, many potential nanotube applications have been investigated, including storage and energy conversion devices, sensors, semiconductors in nanoscale molecular sieves, hydrogen storage materials, additives for polymeric bracket materials in catalytic processes, etc [6]. However, many of these applications have yet to be analyzed and tested properly, although some have already reached the industrial production phase [6]. For this reason, for the large-scale preparation of CNTs, a variety of synthetic strategies have been recently developed and extended to inorganic materials, such as zinc oxide [7–9], titanium dioxide [10,11], aluminum nitride [12], boron nitride [13–15], and other systems [16–19]. In some cases, nanotubes of inorganic materials may be more advantageous than SWCNTs, owing to their interesting qualities and well-established properties, which can provide new scientific and technological perspectives.

The strong chemical similarities between SWCNTs and graphene enable to apply the research experience and relevant methodologies developed for graphene to inorganic nanotubes [20].

In particular, CNT electronic properties sensitively depend on the diameter and chiral angle, i.e., slight differences in these parameters can cause significant changes in the material, such as that from metallic to semiconductor. Previous studies based on scanning tunneling microscopy [21,22] and performed at a large energy scale (~2 eV) confirmed the prediction that CNTs can be semiconducting or metallic depending on the tube diameter and the chiral angle between the tube axis and hexagon rows in the atomic lattice [23,24]. Specifically, armchair SWCNTs are always metallic, while zigzag and chiral nanotubes can be metallic or semiconducting [25], despite the metallic character of the carbon monolayer surface (graphene) [26].

As for graphene, nanotubes without band gap have restricted its application in electronics and, consequently, they are not suitable for semiconducting devices. Therefore, several ways to replace materials with such limitations have been studied in the last years.

Except for the nanotube diameter, no other geometric restrictions are present; however, it was believed that a nanotube could collapse and break when it reaches a diameter of ~25 Å. This collapse is linked to the short curvature of the tube [27]. Nevertheless, several experimental techniques are available to control

* Corresponding author.

http://dx.doi.org/10.1016/j.jssc.2016.01.017
0022-4596/

the nanotube diameter and obtain SWCNTs with diameters up to 30 Å as well as multiwall CNTs with diameters of at least 1000 Å [28–31].

Owing to the close structural similarity between SWCNTs and single-walled ZnO nanotubes (SWZnONTs), the latter can provide new scientific perspectives to technological applications. The ZnO (0001) monolayer surface, which is formed by hexagons of Zn and O atoms with alternate vertices and has the same symmetry and structure observed in graphene sheets, is preferentially used to obtain SWZnONTs by adopting the conventional experimental methods [32,33]. This surface is polar, although the polarity disappears when it is rolled up. The formed nanotubes appear to be promising materials for application in the nanotechnology fields.

Until now, many methods to synthesize ZnO nanotubes have been reported, including thermal reduction [34], vapor phase growth [35], hydrothermal growth [36,37], gas-solid processes [38], sol-gel processes [39], plasma-aided molecular beam epitaxy [40], and metal organic chemical vapor deposition [41]. All ZnO nanotubes are grown with large diameter and thickness.

For instance, Zhang et al. [41] reported the formation of SWZnONTs by the metal organic chemical vapor deposition technique at moderate temperature, 350–450 °C. The obtained nanotubes were grown epitaxially on (0001) sapphire substrates, with both the ZnO *c*-axis and growth direction parallel to the substrate normal. All nanotubes had a hexagonal cross section and the same in-plane orientation. The well-defined hexagonal shape is an indication of epitaxial growth and, consequently, reveals the single-crystal nature of the tubes. According to Shen et al. [42], SWZnONTs with small diameters are more stable than nanowires or nanobelts, but become less stable if the diameter exceeds that of the (24,0) nanotube. Furthermore, Zhou and coworkers [43] studied the size-and-surface dependent stability of (8,0) SWZnONTs, observing a good surface texture. Rout et al. [44] explored the application of SWZnONTs as solar cells, photomicrocavities (owing to the hexagonal nature), and hydrogen and ethanol gas sensors.

In addition, Tu and Hu, [45] using density functional theory (DFT) calculations, found that the piezoelectric behavior of the SWZnONTs strongly depended on their chirality, and also obtained negative values of the binding energy (BE) in all the analyzed models. The strong dependence between structure, electronic profiles, and thermodynamic stability of the ZnO nanotube wall thickness was studied by Xu et al. [46] at the Generalized Gradient Approximation (GGA) level of theory; the close relationship between the band gap energy, $E_{gap}$, and the BE values was found to be inversely proportional to the number of zigzag edge configurations.

As many of these theoretical studies have shown considerably different results, this research topic is clearly still open and indefinite. Furthermore, several published works focused on models based on SWZnONTs with small diameters. Nevertheless, one-dimensional nanostructures have atomic order limited to the nanoscale thus, the use of theoretical quantum chemical calculations and more realistic theoretical models that can support the experimental findings are crucial to achieve an accurate understanding of the related phenomena. Theoretical chemistry methods are widely recognized as complementary tools for the interpretation of experimental data, and can help predict new results and practical strategies.

This paper discusses the structural and electronic properties of SWZnONTs with three different nanotube arrangements (armchair, zigzag, and chiral) and various diameters and chiral angles, based on the periodic DFT formalism.

The research in SWNTs arises from the variety of nanotube diameters and chiral angles, which can significantly affect the structural and electronic properties, showing an ensemble of features that can complicate the foresight of possible technological applications.

The electronic properties were evaluated by analyzing the band gap energies, band structures, density of states (DOS), and density and electrostatic charge maps. The strain ($E_{strain}$) and formation ($E_{form}$) energies, which are not usually available as experimental data, were calculated to estimate its preferential formation. Thus, these theoretical findings may provide a rational development for designing of new nanoelectronic devices.

The results were compared with similar calculated properties of SWCNTs at the same computational level and formalism, as well as with data available in the literature.

## 2. Computing method and models

The theoretical simulations of SWZnONTs and SWCNTs were performed by using periodic DFT with standard hybrid B3LYP functional [47] and the CRYSTAL14 software [48].

CRYSTAL14 uses a Gaussian-type basis set to represent crystalline orbitals as a linear combination of Bloch functions defined in terms of local functions (atomic orbitals). An overview of the algorithms used in the introduction of the DFT into the CRYSTAL computer code is presented by Tawler and coworkers [49].

The usually B3LYP functional is described by the following equation:

$$E_{XC}^{B3LYP}=E_{X}^{LDA}+0.20\left(E_{X}^{HF}-E_{X}^{LDA}\right)+0.72\left(E_{X}^{GGA}-E_{X}^{LDA}\right)+E_{C}^{LDA}+0.81\left(E_{C}^{GGA}-E_{C}^{LDA}\right) \quad (1)$$

In contrast to the generally used B3LYP, the CRYSTAL code uses the local functional fitted to the accurate correlation energy of the uniform electron gas (Vosko–Wilk–Nusair-5) [50], which is used to extract the local part of LYP correlation potential.

Hybrid density functionals have been extensively applied to provide accurate descriptions of crystalline structures. In particular, this functional has been successfully employed to investigate electronic and structural properties in previous works [51–53]. However, other three different functional were adopted for test: PWGGA [54], PBE0 [55], and HSE06 [56]. Upon analysis of the calculated structural and electronic properties of bulk, surface and nanotube, the functional B3LYP showed the best results.

The zinc, oxygen, and carbon atom centers were described by all-electron Gaussian basis sets: 86-411d31G [57] for zinc, 8-411d1 [58] for oxygen, and 6–21 G* [59] for carbon atoms. A very large grid with 99 radial points and 1454 angular points was adopted. The accuracy of the truncation criteria for bio-electronic integrals (Coulomb and HF exchange series) was controlled by a set of five thresholds ($10^{-10}$, $10^{-10}$, $10^{-10}$, $10^{-20}$, $10^{-40}$). These parameters represent the overlap and penetration for Coulomb integrals, the overlap for HF exchange integrals, and the pseudo-overlap (HF exchange series), respectively.

The DOS, and band structure were analyzed using the Properties14 routine implemented in the CRYSTAL code, employing the same *k*-point sampling as the diagonalization of the Fock matrix for the optimization process. The charge and electrostatic potential difference maps were built using the isolated atoms as references, taking isolines at $\pm 0.001$ |e|/Å. This analysis is useful to infer on the difference of covalent and ionic character between SWZnONTs and SWCNTs.

The ZnO wurtzite structure has a direct wide band gap of 3.37 eV [60] and belongs to the space group $P6_3mc$ with two Bravais lattice ($a=3.258$ Å, $c=5.220$ Å) [61] and one internal coordinate $u=0.382$ [61]. Its structure can be depicted as a zinc atom surrounded by four oxygen atoms with $sp^3$-hybridization in a tetrahedron configuration along the *c*-axis, producing an accumulating normal dipole moment. We have previously studied this

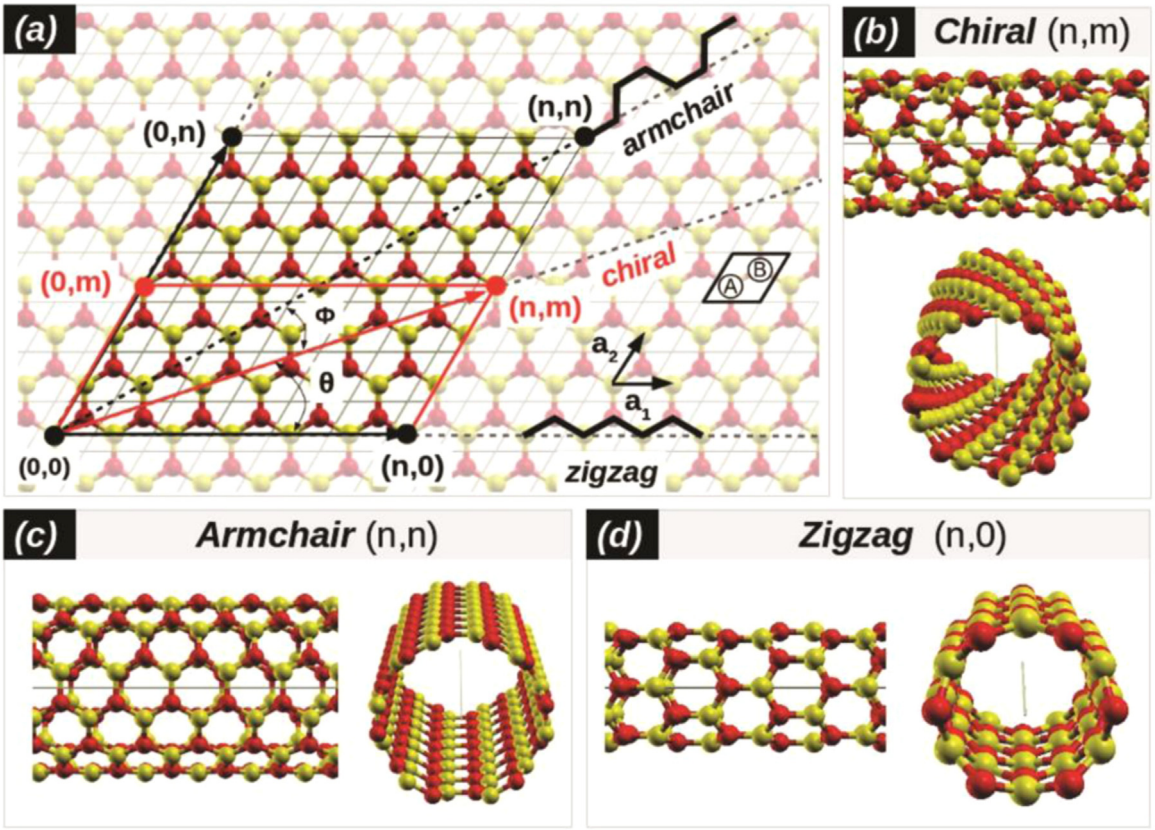


**Fig. 1.** Scheme for generic single-walled nanotube construction (a) from a monolayer surface forming structures with (b) chiral (*n*,*m*), (c) armchair (*n*,*n*), and (d) zigzag (*n*,0) symmetries.

system in several configurations, including surfaces [62] and bulk disorder [63,64].

The graphite structure consists of flat layers of hexagons of carbon atoms. In each layer, i.e., in a graphene sheet, the $sp^2$-hybridized carbon atoms are covalently bonded to three other carbon atoms. Graphite belongs to the space group $P6_3/mmc$ with unit cell parameters $a=2.456$ Å and $c=6.696$ Å, and one adimensional internal coordinate $u=0.250$ [65].

As a first step for the construction of the nanotube models, the optimizations of the lattice parameters and internal coordinates of ZnO and graphite were conducted to minimize the total energy. Second, ZnO (0001) monolayer surface and graphene were built from the optimized bulk parameters and reoptimized in function of the coordinates. From this relaxed surface, SWNTs were constructed (see Fig. 1). Depending on the direction of the rolling sheet, the nanotubes can be classified as armchair (*n*, *n*), zigzag (*n*, 0), and chiral nanotubes (*n*, *m*), where the integers *n* and *m* determine the diameter and chirality of the nanotube (Fig. 1).

For SWCNTs, $E_{gap}$ is heavily influenced by the values of *n* and *m*; as mentioned above, all armchair nanotubes present a metallic character, whereas the zigzag and chiral nanotubes can be metallic or semiconductor depending on their chirality. Theoretically, the rule $n - m=3k$ [21] allows foreseeing the electronic behavior of the nanotube. However, for nanotubes with a small diameter, the rule is not applicable, owing to the interactions present in the cavity; for example, the (5,0) zigzag nanotube should be a semiconductor, but it has indeed a metallic character due to its small diameter (~5 Å).

For armchair and zigzag nanotubes, $n=5$, 10, 15, 20, 50, and 100 was selected. The chiral nanotubes were divided into four *m*-sets, $m=3$, 4, 5, and 10, with $m < n \leq 2m$ with for $n=4$, 5, 6,…, 20. When $m=10$, the values of *n* are between 11 and 20. These models were adopted by their similar large diameter in comparison with armchair and zigzag nanotubes. In total, six armchair, six zigzag, and twenty one chiral nanotubes were constructed.

The number of atoms in a single nanotube can be determined by the Eq. (2), while its structure is determined by means of the chiral vector $\vec{R}=n\vec{a}_1+m\vec{a}_2$ in the unrolled sheet, where $\vec{a}_1$ and $\vec{a}_2$ are base vectors. In addition, the chiral nanotube angle ($\theta$) is defined as the angle between the $\vec{R}$ and $\vec{a}_1$ vectors [48,66] (Fig. 1). From $\vec{R}$, the nanotube diameter ($D$) and $\theta$ can be calculated as Eqs. (3) and (4):

$$4\left(n^2 + nm + m^2\right)\cdot gcd^{-1}(2n + m, 2m + n) \tag{2}$$

$$D=\sqrt{3}\,d\frac{\sqrt{n^2 + nm + m^2}}{\pi}, \tag{3}$$

$$\theta = \tan^{-1}\left(\sqrt{3}\frac{m}{2n + m}\right) \tag{4}$$

where $d$ is the Zn–O, or C–C, bond length. The armchair and zigzag chiral angles are fixed at 30° and 0°, respectively, whereas, for chiral nanotubes, $\theta$ can change as a function of the *n* and *m* values. Notably, $E_{strain}$ is calculated according to the equation $E_{strain}=(E_{NT}\cdot n_{NT}{}^{-1})-E_{(0001)}$, where $E_{(0001)}$ is the surface energy, $E_{NT}$ is the energy of the nanotube, and $n_{NT}$ is the number of atoms in the nanotube. As $E_{strain}$ includes the energy necessary to "wrap" a nanotube from the surface, lower $E_{strain}$ values facilitate the fabrication of the nanotube. On the other hand, $E_{form}$ is the energy of the nanotube obtained from the bulk, and can be calculated from $E_{form}=(E_{NT}\cdot n_{NT}{}^{-1})-E_{bulk}\, n_{bulk}{}^{-1}$, where $E_{bulk}$ is the energy of the bulk and $n_{bulk}$ is the number of atoms in the bulk.

## 3. Results and discussion

### 3.1. Nanotube geometry

For ZnO, the optimized calculated parameters were $a=3.274$ Å, $c=5.250$ Å, and $u=0.383$, corresponding to a deviation of 0.57%, 0.20%, and 0.26%, respectively, from the experimental values; $E_{gap}$ was calculated as 3.21 eV. All results were in good agreement with the experimental values [60,61] and other theoretical works [67]. The optimized lattice parameters for the graphite structure were $a=2.451$ Å, $c=6.559$ Å, and $u=0.250$, showing a deviation 0.20%, 2.04%, and 0.0%, respectively, from the experimental values [61].

Tables 1 and 2 report the theoretical optimized diameter, nanotube length, Zn–O (C–C) average bond length, Zn–O–Zn (C–C–C) average bond angle, overlap population, Mulliken charges, $E_{gap}$, $E_{strain}$ and $E_{form}$ of SWZnONTs and SWCNTs, respectively.

According to the data in Tables 1 and 2, the armchair and zigzag nanotubes had the same number of atoms, which increased with $n$ and $m$; conversely, in chiral nanotubes, the number of atoms was not proportional to $n$ and $m$. For this reason, obtaining a direct relationship in chiral nanotubes is more complicated. The analysis of the geometrical structure of SWZnONTs showed that the calculated Zn–O bond length was ~1.89 Å, whereas the Zn–O–Zn bond angle was 119°. The (5,0) SWZnONT exhibited the smallest diameter, length, bond length, bond angle, and overlap of all simulated nanotubes, including the chiral nanotube (4,3), which had the most similar diameter.

The increase in diameter of the SWZnONTs results in bond lengths and bond angles very similar to those of the calculated (0001) monolayer surface. This structural similarity was also observed in the following studies. Lacivita et al. [67] analyzed armchair SWZnONTs from (4,4) to (50,50), and showed that the Zn–O bond length of the (50,50) nanotube was 1.89 Å, identical to that of the monolayer (1.89 Å), in agreement with the results presented in this work. Zhou and coworkers reported SWZnONT zigzag structures that were very similar to the (0001) surface and to those of CNTs. Wang et al. [68] also predicted the same behavior for SWZnONTs with different chiralities. SWZnONTs with chiral structures (4,2), (4,3), (5,3), (6,3), and (7,3) were studied by Zhang et al.[69] by using the DFT formalism with the GGA functional. These authors calculated the Zn–O bond length in the range of 1.908–1.926 Å.

The SWCNT geometrical structures were also analyzed; the results are reported in Table 2. All armchair, zigzag, and chiral nanotubes exhibited a geometrical structure similar to the (0001) monolayer surface, with average C–C bond length of 1.43 Å and bond angle of ~120° (Table 2). Even the smallest nanotubes, (4,3), (5,5) and (5,0), showed a geometry resembling those of the surface and bulk, as the bond lengths and angles of bulk and surface do not differ significantly. These results were in good agreement with the findings of Imtani and coworkers [70], who analyzed chiral nanotubes with a fixed chirality ($\boldsymbol{m}/\boldsymbol{n}$), obtaining a geometry similar to that of graphene.

**Table 1**

Number of atoms in the nanotube ($n_{NT}$), nanotube diameter (D; Å), nanotube length ($|\vec{L}|$; Å), average Zn–O bond length (Å), overlap population (m|e|), average Zn–$\hat{O}$–Zn bond angle (degrees), Mulliken charges, band gap energy ($E_{gap}$; eV), strain energy ($E_{strain}$; eV/atom), and formation energy ($E_{form}$; eV/atom) of SWZnONTs.

| | $n_{NT}$ | D | θ | $\lvert\vec{L}\rvert$ | Zn–O (Overlap) | Zn–$\hat{O}$–Zn | Q | $E_{gap}$ | $E_{strain}$ | $E_{form}$ |
|---|---|---|---|---|---|---|---|---|---|---|
| **Armchair** | | | | | | | | | | |
| (5,5) | 20 | 9.03 | 30.0 | 3.26 | 1.88(195) | 118.83 | 0.883 | 4.46 | 0.03 | 0.43 |
| (10,10) | 40 | 18.05 | 30.0 | 3.26 | 1.89 (197) | 119.79 | 0.885 | 4.52 | 0.01 | 0.40 |
| (15,15) | 60 | 27.08 | 30.0 | 3.26 | 1.89 (197) | 119.86 | 0.885 | 4.53 | 0.00 | 0.40 |
| (20,20) | 80 | 36.11 | 30.0 | 3.26 | 1.89 (197) | 119.94 | 0.885 | 4.54 | 0.00 | 0.40 |
| (50,50) | 200 | 90.27 | 30.0 | 3.26 | 1.89 (197) | 119.98 | 0.885 | 4.54 | 0.00 | 0.40 |
| (100,100) | 400 | 180.54 | 30.0 | 3.26 | 1.89 (197) | 119.99 | 0.885 | 4.54 | 0.00 | 0.40 |
| **Zigzag** | | | | | | | | | | |
| (5,0) | 20 | 5.21 | 0.0 | 5.67 | 1.87 (189) | 112.95 | 0.883 | 4.32 | 0.11 | 0.51 |
| (10,0) | 40 | 10.42 | 0.0 | 5.67 | 1.89 (195) | 118.77 | 0.884 | 4.49 | 0.02 | 0.42 |
| (15,0) | 60 | 15.64 | 0.0 | 5.67 | 1.89 (196) | 119.14 | 0.885 | 4.52 | 0.01 | 0.41 |
| (20,0) | 80 | 20.85 | 0.0 | 5.67 | 1.89 (197) | 119.80 | 0.885 | 4.53 | 0.01 | 0.40 |
| (50,0) | 200 | 52.12 | 0.0 | 5.67 | 1.89 (197) | 119.96 | 0.885 | 4.54 | 0.00 | 0.40 |
| (100,0) | 400 | 104.23 | 0.0 | 5.67 | 1.89 (197) | 120.00 | 0.885 | 4.54 | 0.00 | 0.40 |
| **Chiral** | | | | | | | | | | |
| (4,3) | 148 | 6.34 | 25.29 | 34.50 | 1.88 (194) | 117.67 | 0.882 | 4.38 | 0.07 | 0.46 |
| (5,3) | 196 | 7.30 | 21.79 | 39.70 | 1.88 (195) | 118.18 | 0.883 | 4.42 | 0.05 | 0.45 |
| (6,3) | 84 | 8.27 | 19.11 | 15.03 | 1.89 (195) | 118.56 | 0.883 | 4.45 | 0.04 | 0.43 |
| (5,4) | 244 | 8.14 | 49.11 | 44.52 | 1.89 (195) | 118.53 | 0.883 | 4.44 | 0.04 | 0.43 |
| (6,4) | 152 | 9.09 | 23.41 | 24.80 | 1.89 (195) | 118.81 | 0.883 | 4.46 | 0.03 | 0.43 |
| (7,4) | 124 | 10.05 | 21.05 | 18.26 | 1.89 (195) | 119.01 | 0.884 | 4.48 | 0.03 | 0.42 |
| (8,4) | 112 | 11.03 | 19.11 | 15.01 | 1.89 (196) | 119.18 | 0.884 | 4.49 | 0.02 | 0.42 |
| (6,5) | 364 | 9.94 | 26.99 | 54.11 | 1.89 (195) | 118.60 | 0.879 | 4.53 | 0.02 | 0.41 |
| (7,5) | 436 | 10.88 | 24.50 | 59.22 | 1.89 (195) | 118.79 | 0.880 | 4.53 | 0.02 | 0.41 |
| (8,5) | 172 | 11.84 | 22.44 | 21.47 | 1.89 (196) | 119.21 | 0.881 | 4.53 | 0.01 | 0.41 |
| (9,5) | 604 | 12.81 | 20.63 | 69.70 | 1.89 (196) | 119.35 | 0.881 | 4.53 | 0.01 | 0.41 |
| (10,5) | 140 | 13.79 | 19.11 | 15.01 | 1.89 (196) | 119.42 | 0.882 | 4.53 | 0.01 | 0.41 |
| (11,10) | 1324 | 18.96 | 28.43 | 103.19 | 1.89 (197) | 119.72 | 0.883 | 4.53 | 0.01 | 0.40 |
| (12,10) | 728 | 19.89 | 26.99 | 54.11 | 1.89 (197) | 119.73 | 0.884 | 4.54 | 0.01 | 0.40 |
| (13,10) | 532 | 20.82 | 25.69 | 37.77 | 1.89 (197) | 119.77 | 0.884 | 4.54 | 0.01 | 0.40 |
| (14,10) | 872 | 21.77 | 24.50 | 59.22 | 1.89 (197) | 119.78 | 0.884 | 4.54 | 0.01 | 0.40 |
| (15,10) | 380 | 22.72 | 23.41 | 24.72 | 1.89 (197) | 119.80 | 0.884 | 4.54 | 0.00 | 0.40 |
| (16,10) | 344 | 23.68 | 22.41 | 21.47 | 1.89 (197) | 119.82 | 0.884 | 4.54 | 0.00 | 0.40 |
| (17,10) | 2236 | 24.64 | 21.49 | 134.11 | 1.89 (197) | 119.83 | 0.884 | 4.54 | 0.00 | 0.40 |
| (18,10) | 1208 | 25.62 | 20.63 | 69.70 | 1.89 (197) | 119.85 | 0.884 | 4.54 | 0.00 | 0.40 |
| (19,10) | 868 | 26.60 | 19.84 | 48.24 | 1.89 (197) | 119.88 | 0.884 | 4.54 | 0.00 | 0.40 |
| (20,10) | 280 | 27.58 | 19.11 | 15.01 | 1.89 (197) | 119.90 | 0.884 | 4.54 | 0.00 | 0.40 |

**Table 2**

Number of atoms in the nanotube ($n_{NT}$), nanotube diameter (D; Å), nanotube length ($|\vec{L}|$; Å), average C–C bond length (Å),overlap population (mle), average C–$\hat{C}$–C bond angle, Mulliken charges, band gap energy ($E_{gap}$; eV), strain energy ($E_{strain}$; eV/atom), and formation energy ($E_{form}$; eV/atom) of SWCNTs.

| | $n_{NT}$ | D | $\theta$ | $\|\vec{L}\|$ | C-C (Overlap) | C-$\hat{C}$-C | Q | $E_{gap}$ | $E_{strain}$ | $E_{form}$ |
|---|---|---|---|---|---|---|---|---|---|---|
| **Armchair** | | | | | | | | | | |
| (5,5) | 20 | 6.76 | 30.0 | 2.45 | 1.43 (446) | 118.93 | 0.0 | 0.07 | 0.19 | −0.58 |
| (10,10) | 40 | 13.51 | 30.0 | 2.45 | 1.43 (444) | 119.30 | 0.0 | 0.04 | 0.05 | −0.72 |
| (15,15) | 60 | 20.27 | 30.0 | 2.45 | 1.43 (440) | 119.82 | 0.0 | 0.04 | 0.02 | −0.75 |
| (20,20) | 80 | 27.03 | 30.0 | 2.45 | 1.43 (438) | 119.97 | 0.0 | 0.05 | 0.01 | −0.76 |
| (50,50) | 200 | 67.57 | 30.0 | 2.45 | 1.43 (436) | 119.99 | 0.0 | 0.07 | 0.00 | −0.76 |
| (100,100) | 400 | 135.15 | 30.0 | 2.45 | 1.43 (435) | 120.00 | 0.0 | 0.07 | 0.00 | −0.77 |
| **Zigzag** | | | | | | | | | | |
| (5,0) | 20 | 3.90 | 0.0 | 4.26 | 1.42 (446) | 117.02 | 0.0 | 0.0 | 0.61 | −0.15 |
| (10,0) | 40 | 7.78 | 0.0 | 4.26 | 1.43 (444) | 119.20 | 0.0 | 1.19 | 0.14 | −0.63 |
| (15,0) | 60 | 11.70 | 0.0 | 4.26 | 1.43 (440) | 119.64 | 0.0 | 0.17 | 0.06 | −0.70 |
| (20,0) | 80 | 15.61 | 0.0 | 4.26 | 1.43 (440) | 119.80 | 0.0 | 0.68 | 0.04 | −0.73 |
| (50,0) | 200 | 39.01 | 0.0 | 4.26 | 1.43 (436) | 119.96 | 0.0 | 0.27 | 0.01 | −0.76 |
| (100,0) | 400 | 78.03 | 0.0 | 4.26 | 1.43 (436) | 119.99 | 0.0 | 0.14 | 0.00 | −0.76 |
| **Chiral** | | | | | | | | | | |
| (4,3) | 148 | 4.78 | 25.29 | 26.05 | 1.43 (440) | 117.78 | 0.0 | 2.08 | 1.12 | 0.36 |
| (5,3) | 196 | 5.46 | 21.79 | 29.92 | 1.43 (444) | 118.36 | 0.0 | 2.01 | 1.04 | 0.28 |
| (6,3) | 84 | 6.19 | 19.11 | 10.30 | 1.43 (445) | 118.80 | 0.0 | 0.11 | 0.99 | 0.22 |
| (5,4) | 244 | 6.09 | 49.11 | 38.92 | 1.43 (436) | 118.74 | 0.0 | 1.69 | 0.99 | 0.22 |
| (6,4) | 152 | 6.80 | 23.41 | 18.64 | 1.43 (446) | 118.93 | 0.0 | 1.60 | 0.95 | 0.18 |
| (7,4) | 124 | 7.53 | 21.05 | 13.75 | 1.43 (445) | 119.13 | 0.0 | 0.02 | 0.92 | 0.15 |
| (8,4) | 112 | 8.26 | 19.11 | 11.32 | 1.43 (446) | 119.28 | 0.0 | 1.19 | 0.89 | 0.12 |
| (6,5) | 364 | 7.50 | 26.99 | 40.81 | 1.43 (446) | 119.11 | 0.0 | 1.40 | 0.92 | 0.15 |
| (7,5) | 436 | 8.21 | 24.50 | 44.64 | 1.43 (446) | 119.26 | 0.0 | 1.33 | 0.89 | 0.13 |
| (8,5) | 172 | 8.93 | 22.44 | 16.19 | 1.42 (446) | 119.37 | 0.0 | 0.02 | 0.88 | 0.11 |
| (9,5) | 604 | 9.66 | 20.63 | 52.56 | 1.42 (445) | 119.46 | 0.0 | 1.05 | 0.86 | 0.09 |
| (10,5) | 140 | 10.40 | 19.11 | 11.31 | 1.43 (444) | 119.54 | 0.0 | 1.05 | 0.85 | 0.08 |
| (11,10) | 1324 | 14.30 | 28.43 | 77.82 | 1.43 (442) | 119.75 | 0.0 | 0.72 | 0.81 | 0.04 |
| (12,10) | 728 | 15.00 | 26.99 | 47.21 | 1.43 (442) | 119.77 | 0.0 | 0.69 | 0.81 | 0.04 |
| (13,10) | 532 | 15.70 | 25.69 | 28.48 | 1.43 (441) | 119.79 | 0.0 | 0.02 | 0.81 | 0.04 |
| (14,10) | 872 | 16.41 | 24.50 | 44.66 | 1.43 (441) | 119.81 | 0.0 | 0.62 | 0.80 | 0.03 |
| (15,10) | 380 | 17.13 | 23.41 | 18.64 | 1.43 (440) | 119.82 | 0.0 | 0.61 | 0.80 | 0.03 |
| (16,10) | 344 | 17.86 | 22.41 | 16.19 | 1.43 (440) | 119.84 | 0.0 | 0.02 | 0.80 | 0.03 |
| (17,10) | 2236 | 18.64 | 21.49 | 101.13 | 1.43 (439) | 119.84 | 0.0 | 0.82 | 0.79 | 0.03 |
| (18,10) | 1208 | 19.32 | 20.63 | 52.56 | 1.43 (439) | 119.86 | 0.0 | 0.53 | 0.79 | 0.03 |
| (19,10) | 868 | 20.06 | 19.84 | 36.38 | 1.43 (439) | 119.87 | 0.0 | 0.02 | 0.79 | 0.03 |
| (20,10) | 280 | 20.65 | 19.11 | 11.32 | 1.43 (439) | 119.88 | 0.0 | 0.49 | 0.79 | 0.02 |

### 3.2. Strain energy, formation energy and electronic structures

The analysis of $E_{strain}$ and $E_{form}$ helps predict the preferential chirality formation. Fig. 2 illustrates the relationship between $E_{strain}$, $E_{form}$, and $E_{gap}$ as functions of the diameter for SWZNONTs and SWCNTs with different chiralities. It is important notice that the $E_{strain}$ and $E_{form}$ not allow comparisons of stabilities order as a function of diameter and chirality.

The increase of SWZnONT nanotube diameter showed a decrease in $E_{strain}$ and $E_{form}$ and renders a convergence from (15,15) and (20,0) nanotubes. Both energies had the same calculated value and identical behavior for equivalent nanotube diameters; however, comparing the number of atoms in the nanotube, the energies of the zigzag nanotubes were slightly higher than those of the armchair nanotubes by 0.01 eV/atom. This little difference may depend on the methodology or the error accumulation in the numerical calculation process.

In a general sense, $E_{form}$ was higher than $E_{strain}$ for both nanotube types, suggesting that nanotubes are more easily formed from a monolayer surface than from the ZnO bulk. The (5,0) nanotube (first point in Fig. 2c) had the small diameter of 5.21 Å, and exhibited the highest $E_{strain}$ and $E_{form}$ values; this may be caused by the weak interactions between the atoms of the nanotube cavity, which lead to high $E_{strain}$ and low stability.

In the case of the thinnest chiral nanotubes, $E_{strain}$ and $E_{form}$ were greater than those of other chiral nanotubes with the same chiral angle, such as (6,3) and (10,5) ($\theta = 19.11°$); however, $E_{strain}$ of (6,3) and (10,5) was 0.04 eV/atom and 0.01 eV/atom, respectively. These results showed that nanotubes with a small diameter can be more difficult to obtain than those with larger diameters, while retaining the chirality. In general, $E_{strain}$ for chiral nanotubes was 0.01 eV/atom for diameters in the range of 11.84–21.77 Å, while it was equal to zero for diameters in the range of 22.72–27.58, (20,10). However, $E_{form}$ had a value of 0.40 eV/atom in nanotubes with a diameter of 18 Å. Therefore, the three types of SWZnONTs can be formed with the same ease for diameters up to 20 Å.

By increasing the SWCNT diameter, $E_{strain}$ and $E_{form}$ decreased, with $E_{form}$ being smaller than $E_{strain}$. For armchair and zigzag nanotubes, $E_{form}$ was negative, and $E_{strain}$ had positive values; conversely, in chiral SWCNTs, $E_{form}$ had a positive value. Comparing the armchair, zigzag, and chiral nanotubes with diameters of ~20 Å, $E_{strain}$ was equal to 0.02 eV/atom, 0.04 eV/atom, and 0.79 eV/atom, respectively, while $E_{form}$ was equal to −0.75 eV/atom, −0,71 eV/atom, and 0,02 eV/atom, respectively. These results suggest that armchair and zigzag nanotubes are formed almost instantly and more easily than chiral nanotubes.

Comparing $E_{strain}$ of SWZnONTs and SWCNTs with diameters of ~20 Å, the $E_{strain}$ value of the SWZnONTs was smaller than that of the SWCNTs. Similar results were calculated by Zhao and coworkers [71] for aluminum nitride nanotube (AlNNT) using DFT with the PBE functional. These authors concluded that $E_{strain}$ of SWCNTs was greater than that of AlNNTs, gallium nitride nanotubes, and boron nitride nanotubes.

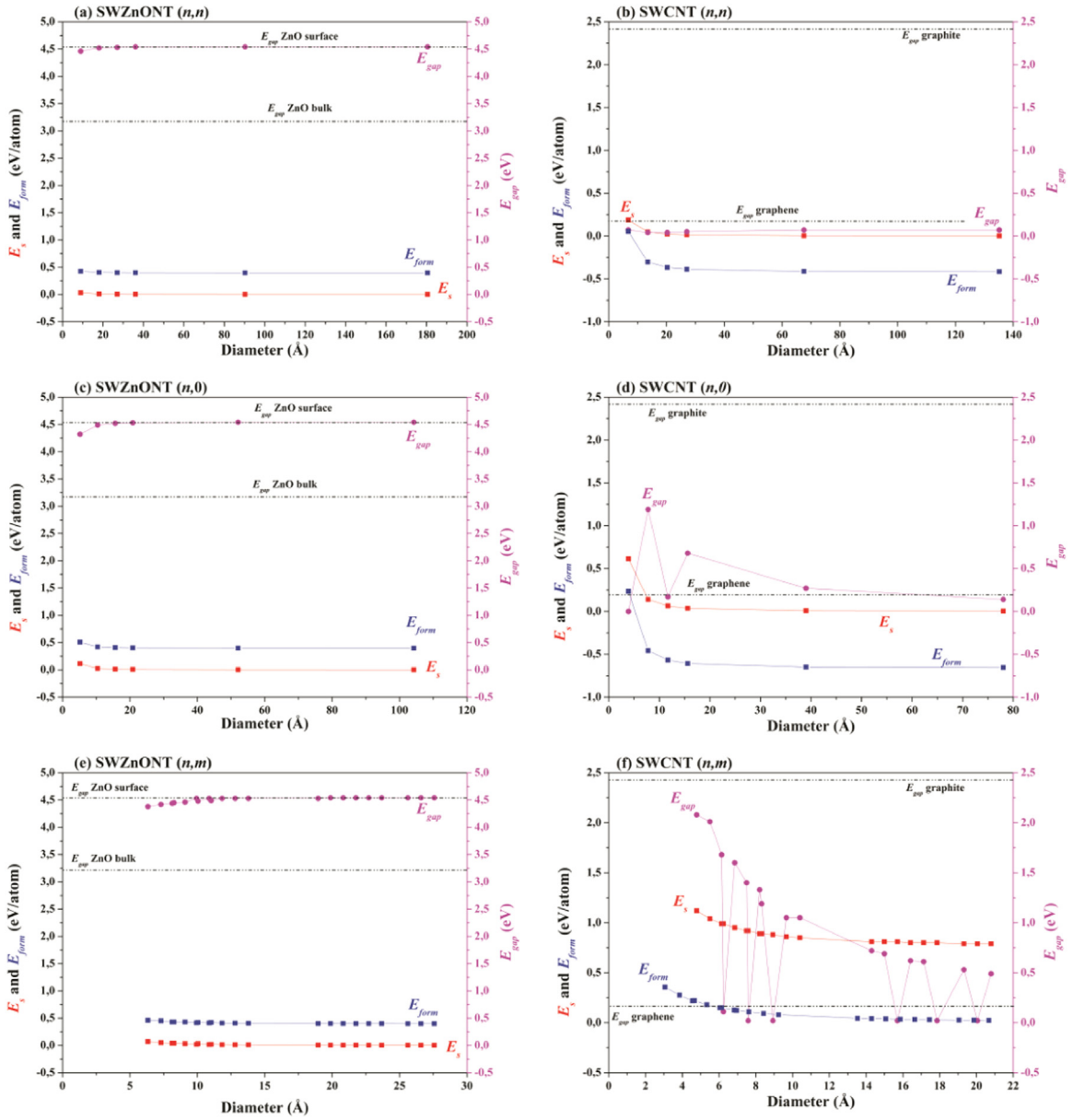


**Fig. 2.** Strain energy (eV/atom) and formation energy (eV/atom) as a function of the diameter (Å) for (a) armchair (*n*,*n*) SWZnONTs, (b) armchair (*n*,*n*) SWCNTs, (c) zigzag (*n*,0) SWZnONTs, (d) zigzag (*n*,0) SWCNTs, (e) chiral (*n*,*m*) SWZnONTs, and (f) chiral (*n*,*m*) SWCNTs.

In general, for nanotubes with small diameters, $E_{form}$ and $E_{strain}$ of the chiral nanotubes were higher than those of armchair and zigzag nanotubes, which lead to, unfavorable obtaining this type of nanotube. This results are in agreement with Wang and coworkers, however, this work analyzes nanotubes with small diameters [68] (less than 20 Å). On the other hand, in the present study, are analyzed the three chiralities with large diameter, and confirmed that the three chiralities can be obtained simultaneously.

An analysis of Fig. 2 shows that, for all SWZnONTs, the increase in diameter led to an increase of $E_{gap}$. The $E_{gap}$ values of armchair and zigzag SWZnONTs (Fig. 2a and c) were in the same range, 4.53 eV, very close to the calculated $E_{gap}$ for the monolayer surface (4.56 eV). The $E_{gap}$ value stabilized for diameters above 20 Å, remaining constant at larger diameters. The $E_{gap}$ values for chiral (*n*,3) and (*n*,4) SWZnONTs (Fig. 2e) showed the same behavior and were smaller than those observed for armchair and zigzag nanotubes. For (*n*,5) and (*n*,10) nanotubes, all calculated $E_{gap}$ values were 4.53 eV and 4,54 eV, respectively, which were in agreement with those calculated for the armchair and zigzag SWZnONTs with large diameters and for the monolayer surface. In general, for large SWZnONTs, the diameter, chirality, and number of atoms do not influence the geometrical structure parameters (bonds and angles), $E_s$, and $E_{gap}$.

The $E_{gap}$ of all SWZnONTs converged to the $E_{gap}$ value of the ZnO monolayer surface, whereas the $E_{gap}$ of the SWCNTs depended on their chirality. All armchair SWCNTs (Fig. 2b) showed a metallic character, with $E_{gap}$ values in the range of 0.04–0.07 eV. On the other hand, $E_{gap}$ of zigzag and chiral SWCNTs (see Table 2 and Fig. 2d–f), according to the rule $\boldsymbol{n} - \boldsymbol{m} = 3\boldsymbol{k}$, was ~0.02 eV and 0.17 eV for (15,0) and (6,3) nanotubes, respectively. However, the (5,0) nanotube, which, according to the rule, should have a semiconductor character, was in fact metallic, in agreement with the studies of Ozgit-Akgun [12]. The curvature effects in nanotubes with a small diameter can strongly influence the electrical properties.

For the other chiral and zigzag SWCNTs, $E_{gap}$ was inversely proportional to the diameter of the nanotube. Thus, for the largest zigzag and chiral nanotubes, the small band gap could be

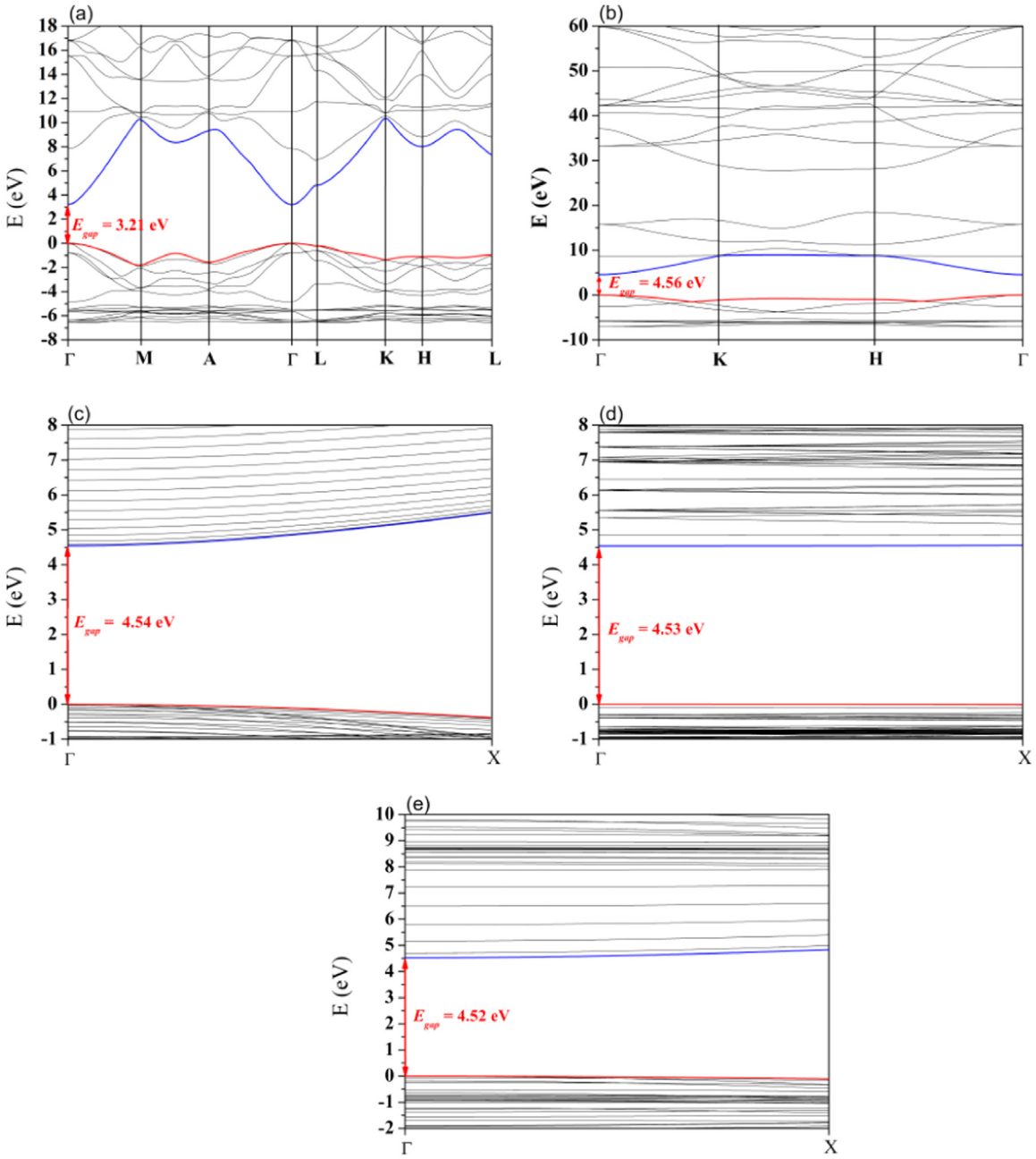


**Fig. 3.** Band structure of (a) bulk, (b) ZnO (0001) surface, (c) (20,20), (d) (15,0), and (e) (8,5) single-walled ZnO nanotubes.

considered as that of a moderate semiconductor. These theoretical results for $E_{gap}$ of SWCNTs are in good agreement with the experimental values reported by Wildöer [21] and colleagues.

However, $E_{gap}$ of SWZnONTs converged to the value of the monolayer surface; this did not occur in SWCNTs, as the graphene has $E_{gap}$ of 0.2 eV.

The band structures and, DOS of SWZnONTs were plotted (50 bands at valence band (VB) and conduct band (CB), respectively, and, the top of the VB coincides with zero energy) and compared with the band structures of bulk and (0001) monolayer surface (Fig. 3).

All band structures of the armchair (Fig. 3c), zigzag (Fig. 3d), and chiral (Fig. 3e) SWZnONTs exhibited a slightly similar behavior, with a direct band gap at the $\Gamma$ point. The bands of zigzag and chiral nanotubes were flatter than those of the armchair tubes. Wang et al. [68], performed the simulations using a double numerical basis set including d-polarization functions with Dmol package and PBE functional. They also obtained direct band gap energy at $\Gamma$ point for the three chiralities; however, the shape of CB for armchair and chiral showed some difference. Another contrast with Wang's workis the decrease of $E_{gap}$ with diameter increase, whereas this work pointed the opposite behavior.However, Zhigang and coworkers [72] also applied Dmol package with BLYP functional and basis set including double zeta quality plus polarization functions, their results are in agreement with the present work. The possible disagreement between Wang, Zhigang and this work is regarding to the applied functional and basis set.

The band gap of the monolayer surface (Fig. 3b), 4.56 eV, also occurred at the $\Gamma$ point, and the bands were more scattered than the bands observed for the nanotubes, which were concentrated near the gap region.

The DOS of the ZnO bulk, monolayer surface, and SWZnONTs are shown in Fig. 4. The analyses of the principal atomic orbital (AO) component of selected bands were performed with a threshold of 0.10 a. u. for the significant eigenvector coefficients.

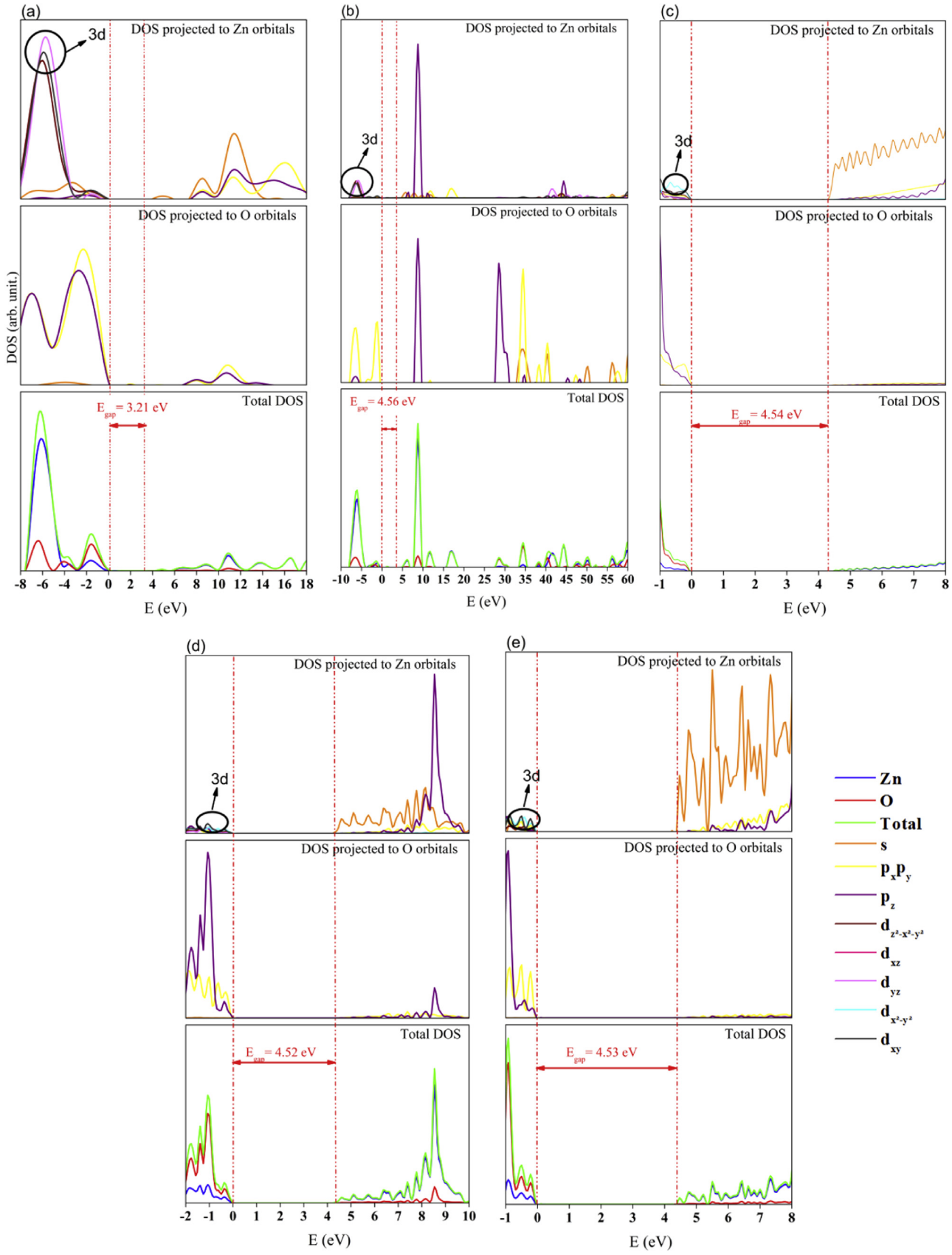


**Fig. 4.** Density of states of (a) bulk, (b) ZnO (0001) surface, (c) (20,20), (d) (15,0), and (e) (8,5) single-walled ZnO nanotubes.

The DOS of bulk and SWZnONTs showed a major contribution from oxygen atoms in the top of the VB and zinc atoms in the conduction band (CB); however, for the monolayer surface, the zinc atoms contributed in both the VB and CB.

The selected AO components for the ZnO bulk and monolayer surface (Fig. 4a and b) indicated that the top of the VB consisted mainly of $2p_xp_y$ orbitals of O atoms and $3d_{yz}$ orbitals of Zn atoms in the approximate region between $-10$ and $-4$ eV. The bottom of the CB had a dominant influence from the s orbitals of Zn atoms for both morphologies, but the $2p_z$ orbitals showed an intense contribution for Zn and O atoms at $\sim$10 eV.

All SWZnONTs (Fig. 4c–e) showed the $p_xp_y$ orbital of Zn and O atoms contributing at VB. In the CB, the s orbital of the Zn atoms was the major contributor. However, the 3d orbitals presented a great contribution in all the VB region, wherein the $3d_{xy}$ and $3d_{x^2-y^2}$ orbitals contributed more significantly; in the (15,0) and (8,5) nanotubes, the $3d_{xy}$ orbitals prevailed, while, in the nanotube (20,20), the $3d_{x^2-y^2}$ orbitals dominated.

The intense peak corresponding to the Zn 3d orbitals is common to all ZnO structures. The uppermost occupied bands assume different shapes depending on the structure. In ZnO bulk, and (0001) monolayer surface, the 3d orbitals presents a peak at $-10$ to $-4$ eV, that corresponds to $3d_{yz}$, and in SWZnONT, the peak appears at $\sim$1 eV. Another correspondence it is about the Zn s orbital, that presents a contribution at CB in all ZnO structure, but in SWZnONT, the peak of Zn s orbitals are more intense than for bulk and surface.

As expected, the band structures of graphite and graphene (Fig. 5a and b) indicated that their band gap is 0 eV, which is in good agreement with other works conducted at different theory levels [73,74]. Their DOS (Fig. 6a and b) showed major contributions from $2p_z$ orbitals, near the top and bottom of the VB and CB, respectively, i.e., in the gap region; in the inner bands, the contribution switched between s and $2p_xp_y$ orbitals.

The band structure for armchair and chiral SWCNTs with $\boldsymbol{n} - \boldsymbol{m}=3\boldsymbol{k}$ (Fig. 5c and d) showed that the top of the VB and

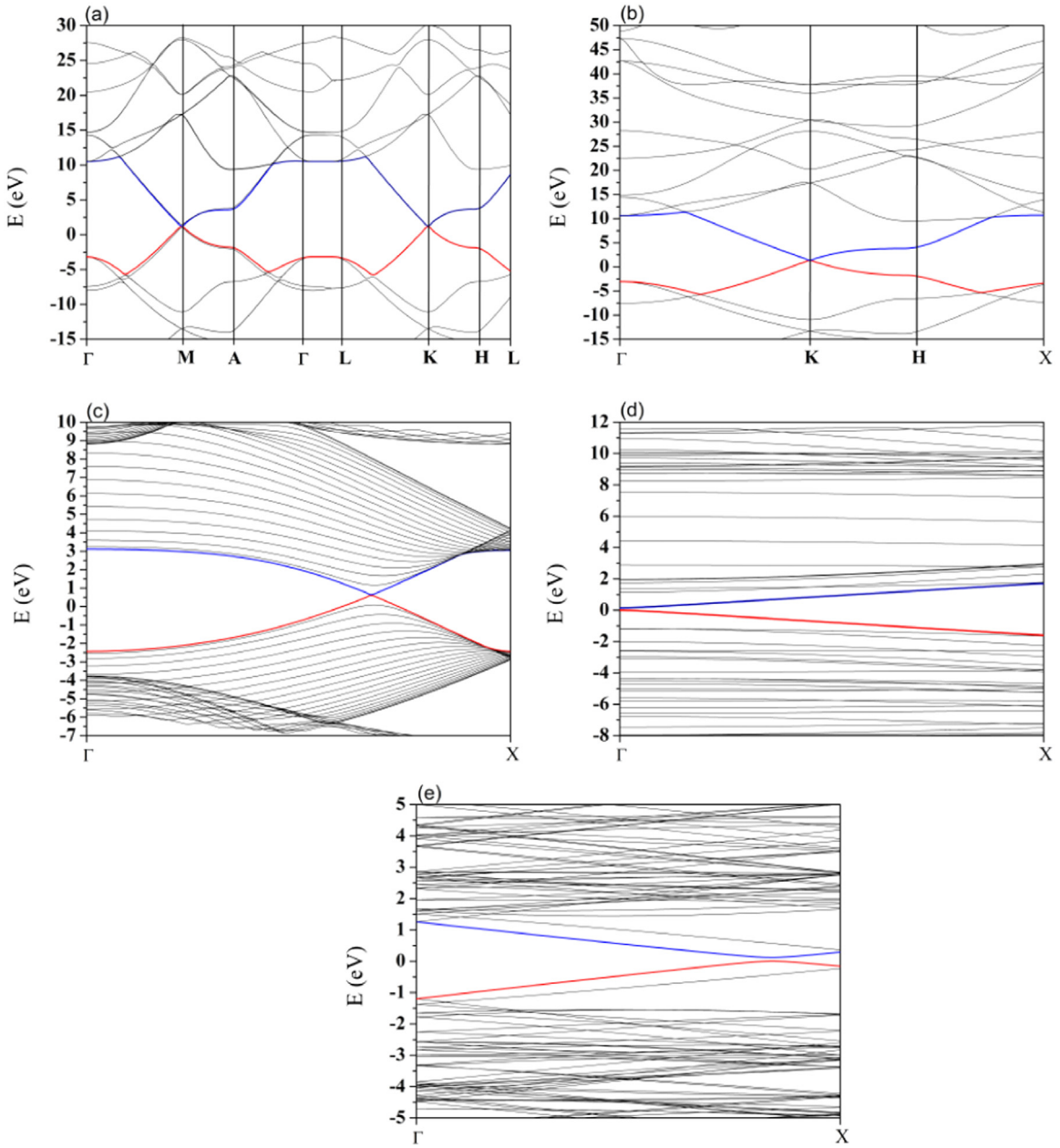


**Fig. 5.** Band structure of (a) graphite, (b) graphene, (c) (20,20), (d) (15,0), (e) (8,5) single-walled carbon nanotubes.

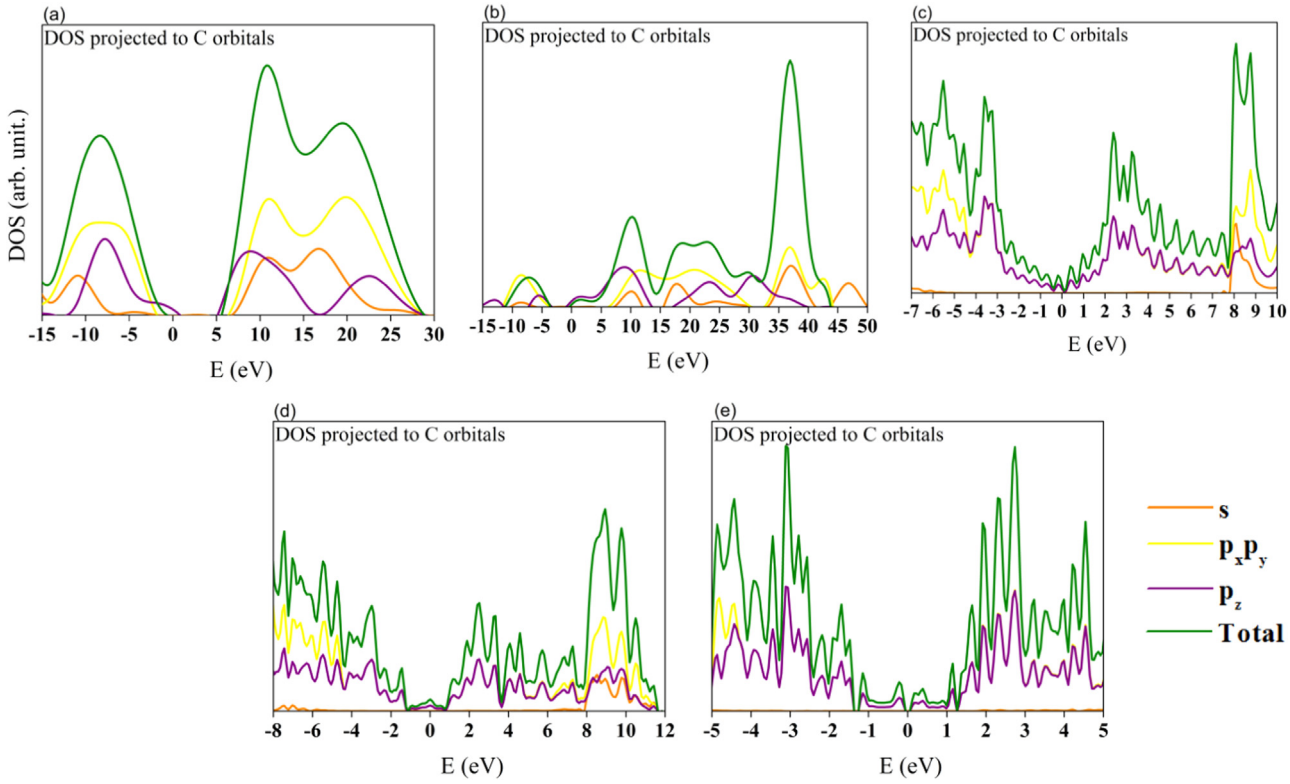


**Fig. 6.** Density of states of (a) graphite, (b) graphene, (c) (20,20), (d) (15,0), (e) (8,5) single-walled carbon nanotubes.

bottom of the CB approached each other, leading to a small $E_{gap}$ between $\Gamma$ and $X$ points (Dirac point), whereas the top of the VB and bottom of the CB in graphite and graphene occurred at the $M$ and $K$ points (Fig. 5b). The band structure of (15,0) nanotubes exhibited direct band gap at the $\Gamma$ point, while, for (5,0), it was between $\Gamma$ and $X$ points. For nanotubes that did not show a metallic character, the band gap occurred at the $\Gamma$ point of ~0.2 eV. The DOS of the SWCNTs (Fig. 6c–e) showed a predominant contribution of $2p_z$ orbitals in all regions, with a small contribution of s and $2p_xp_y$ orbitals in the inner regions of the VB and CB.

The overlap population for SWZnONTs with different chiralities (see Table 1) showed the same value of the (0001) surface, 197 m|e|, when the nanotube diameter increased. However, nanotubes and surface exhibited a stronger chemical bond covalent character than that observed for the ZnO bulk, 143 m|e|.

The SWCNT overlap population analyses exhibited an opposite trend compared with those of the SWZnONTs; by increasing the nanotube diameter, the covalent character decreased, approaching that of graphite and graphene, 435 m|e|.

The electrostatic and charge density maps along the C–C and Zn–O bonds (Figs. 1S and 2S) showed the main difference of polarity between them in each nanotube. Although no significant differences were observed in the bond of each atom pair within the symmetry, compared with CNTs, the ZnO bonds exhibited an ionic character, as mentioned above. In highly strained nanotubes, the bonds tend to become more tensioned and, consequently, more polar. Correspondingly, the band gap changes faster under those conditions.

As a result, in the case of SWZnONTs, $E_{strain}$ and $E_{gap}$ does not depend strongly on ($n$,$m$), but chiral nanotubes with small diameter are more difficult to form (energetically instable); notably, all chiral nanotubes with diameters up to 20 Å can be formed as easily as armchair and zigzag nanotubes, and all are energetically stable. For SWCNTs, $E_{strain}$ does not depend on chirality, but chiral nanotubes are more difficult to obtain; $E_{gap}$ strongly depends on the chirality for zigzag and chiral nanotubes, which can be semiconducting or metallic, depending on their diameter, (5,0), and if the difference between $n$ and $m$ is a multiple of 3. For armchair SWCNTs, $E_{gap}$ remains constant for all diameters. Owing to their properties, SWZnONTs and SWCNTs can be used in photocatalysis, as both present, in all nanotube types, a major contribution from $p_xp_y$ orbitals, which is critical for photocatalysis. However, SWCNTs are organic and only the nanotubes with semiconducting character can be applied, whereas the SWZnONTs can be applied with different chiralities and sizes.

## 4. Conclusions

Gaussian basis set were performed to simulate the structural and electronic properties as well as estimate the $E_{strain}$ and $E_{form}$ values of SWZnONTs and SWCNTs with different chiralities as functions of their diameters.

The simulation results showed that $E_{gap}$, $E_{strain}$, and $E_{form}$ of all SWZnONTs converged to ~4.5 eV, 0.0 eV/atom, and 0.40 eV/atom, respectively, for diameters up to 20 Å, indicating that the chirality is not determinant at large diameters. For all SWZnONTs, $E_{form}$ was larger than $E_{strain}$, suggesting that the nanotubes are formed more easily from the surface than from the bulk.

The analysis of the band structure and DOS of bulk, (0001) monolayer surface, and SWZnONTs showed a direct band gap at the $\Gamma$ points of 3.21 eV, 4.56 eV, and 4.54 eV, respectively, with major contributions from the $p_xp_y$ orbitals of oxygen and zinc atoms in the VB and s orbital of zinc atoms in the CB.

The results obtained in this study are in agreement with the experimental findings, not only from a structural point of view, but also in relation to the electronic properties.

For armchair, zigzag, and chiral SWCNTs, $E_{strain}$ converged to 0.0, 0.0, and 0.79 eV/atom, respectively, and $E_{form}$ to −0.76, −0.77, and 0.02 eV/atom, respectively. Whereas $E_{strain}$ was always positive, $E_{form}$ was negative for armchair and zigzag nanotubes, and

positive for chiral nanotubes. The negative values of $E_{form}$ suggest that SWCNTs are preferentially formed from the bulk and that armchair and zigzag nanotubes are formed almost instantly and more easily than chiral nanotubes. This preferably formation from bulk is expected because the structure of graphite has a layered structure and the ZnO wurtzite structure has a different atomic configuration. In contrast, the graphene has a similar structure of (0001) surface of ZnO.

The band structures of graphite and graphene showed a direct gap at the *K* point, while that of SWCNTs had a direct gap at the $\Gamma$ point for (15,0) and (8,5), but, for all armchair nanotubes, the gap occurred between the $\Gamma$ and *X* points. The DOSs of graphite, graphene, and SWCNTs showed major contributions from $2p_z$ orbitals throughout the entire range under investigation.

Comparing SWCNTs withSWZnONTs, the latter have higher $E_{form}$ than the former, suggesting that they are obtained more easily from the surface, while CNTs can be obtained more easily from the bulk. With respect to the band gap, ZnO nanotubes retain a semiconductor character and their properties are conserved, whereas the carbon nanotube properties depend on the chirality. Therefore, synthesis control is necessary to obtain SWCNTs with desired chirality.

Due to SWZnONTs electronic and optical properties, all chirality of nanotubes with large diameter can be used interchangeably in semiconductor applications.

The methodology and accuracy of our theoretical models from bulk to surfaces and nanotubes is reliable and can be extended and applied to other computational simulations, as doping or adsorption process.

## Acknowledgments

This work is supported by Brazilian Funding Agencies: CNPq, CAPES, FAPESP (2013/19289-0, 2013/19713-7, 2013/07296-2). The computational facilities were supported by resources supplied by Molecular Simulations Laboratory, São Paulo State University, Bauru, Brazil.

## Appendix A. Supplementary material

Supplementary data associated with this article can be found in the online version at http://dx.doi.org/10.1016/j.jssc.2016.01.017.

## References

[1] S. Iijima, Helical microtubeles of graphitic carbon, Nature 354 (1991) 56–58.
[2] E.T. Thostenson, Z.F. Ren, T.W. Chou, Advances in the science and technology of carbon nanotubes and their composites: a review, Compos. Sci. Technol. 61 (2001) 1899–1912.
[3] S. Iijima, T. Ichihashi, Single-shell carbon nanotubes of 1-nm diameter, Nature 364 (1993) 737–737.
[4] D.S. Bethune, C.H. Kiang, M.S. Devries, G. Gorman, R. Savoy, J. Vazquez, R. Beyers, Cobalt-catalyzed growth of carbon nanotubes with single-atomic-layerwalls, Nature 363 (1993) 605–607.
[5] C.H. Kiang, W.A. Goddard, R. Beyers, D.S. Bethune, Carbon nanotubes with single-layer walls, Carbon 33 (1995) 903–914.
[6] R.H. Baughman, A.A. Zakhidov, W.A. de Heer, Carbon nanotubes-the route toward applications, Science 297 (2002) 787–792.
[7] S.B. Kim, S. Kim, S.S. Kwon, W.W. Lee, J.-S. Kim, W.I. Park, Large-scale synthesis of vertically aligned ZnO hexagonal nanotube-rod hybrids using a two-step growth method, J. Am. Ceram. Soc. 96 (2013) 3500–3503.
[8] H. Lu, F. Zheng, M. Guo, M. Zhang, One-step electrodeposition of single-crystal ZnO nanotube arrays and their optical properties, J. Alloy. Compd. 588 (2014) 217–221.
[9] A.B.F. Martinson, J.W. Elam, J.T. Hupp, M.J. Pellin, ZnO nanotube based dye-sensitized solar cells, Nano Lett. 7 (2007) 2183–2187.
[10] R.G. Freitas, M.A. Santanna, E.C. Pereira, Dependence of TiO2 nanotube microstructural and electronic properties on water splitting, J. Power Sources 251 (2014) 178–186.
[11] Z. Gao, Z. Cui, S. Zhu, Y. Liang, Z. Li, X. Yang, Design and synthesis of MWNTs-TiO2 nanotube hybrid electrode and its supercapacitance performance, J. Power Sources 283 (2015) 397–407.
[12] C. Ozgit-Akgun, F. Kayaci, I. Donmez, T. Uyar, N. Biyikli, Template-based synthesis of aluminum nitride hollow nanofibers via plasma-enhanced atomic layer deposition, J. Am. Ceram. Soc. 96 (2013) 916–922.
[13] M. Anafcheh, R. Ghafouri, F. Ektefa, M. Zahedi, Boron-nitride ad-unit and carbon ad-dimer defects in the boron nitride nanotubes, J. Phys. Chem. Solids 79 (2015) 7–13.
[14] N. Zhang, H. Liu, H. Kan, X. Wang, H. Long, Y. Zhou, The influence of metal Mg on micro-morphology and crystallinity of spherical hexagonal boron nitride, Mater. Res. Bull. 68 (2015) 179–184.
[15] N. Zhang, H. Liu, H. Kan, X. Wang, H. Long, Y. Zhou, The Influence of Surface-Active Agent on the Micro-Morphology and Crystallinity of Spherical Hexagonal Boron Nitride, J. Nanosci. Nanotechnol. 15 (2015) 6218–6224.
[16] Y. Duan, J. Zhang, K. Xu, Structural and electronic properties of chiral single-wall copper nanotubes, Sci. China-Phys. Mech. Astron. 57 (2014) 644–651.
[17] E. Chigo Anota, G.H. Cocoletzi, Influence of point defects on the structural and electronic properties of SiC nanotubes, Cent. Eur. J. Chem. 12 (2014) 53–59.
[18] J.-J. Xu, D. Xu, Z.-L. Wang, H.-G. Wang, L.-L. Zhang, X.-B. Zhang, Synthesis of Perovskite-Based Porous La0.75Sr0.25MnO3 Nanotubes as a Highly Efficient Electrocatalyst for Rechargeable LithiumOxygen Batteries, Angew. Chemie-Int. Ed. 52 (2013) 3887–3890.
[19] A. Hosseinian, H.R. Rahimipour, H. Haddadi, A.A. Ashkarran, A.R. Mahjoub, Thermolysis preparation of ZnS nanoparticles from a nano-structure bithiazole zinc(II) coordination compound, J. Mol. Struct. 1074 (2014) 673–678.
[20] C.N.R. Rao, M. Nath, Inorganic nanotubes, Dalton Trans. (2003) 1–24.
[21] J.W.G. Wildoer, L.C. Venema, A.G. Rinzler, R.E. Smalley, C. Dekker, Electronic structure of atomically resolved carbon nanotubes, Nature 391 (1998) 59–62.
[22] T.W. Odom, J.L. Huang, P. Kim, M. Ouyang, C.M. Lieber, Scanning tunneling microscopy and spectroscopy studies of single wall carbon nanotubes, J. Mater. Res. 13 (1998) 2380–2388.
[23] J.W. Mintmire, B.I. Dunlap, C.T. White, Are fullerene tubeles metallic, Phys. Rev. Lett. 68 (1992) 631–634.
[24] R. Saito, M. Fujita, G. Dresselhaus, M.S. Dresselhaus, Electronic-structure of chiral graphene tubules, Appl. Phys. Lett. 60 (1992) 2204–2206.
[25] X. Lu, Z.F. Chen, Curved Pi-conjugation, aromaticity, and the related chemistry of small fullerenes ( < C-60) and single-walled carbon nanotubes, Chem. Rev. 105 (2005) 3643–3696.
[26] H. Hibino, S. Tanabe, S. Mizuno, H. Kageshima, Growth and electronic transport properties of epitaxial graphene on SiC, J. Phys. D-Appl. Phys. 45 (2012).
[27] J. Tersoff, R.S. Ruoff, Structural-properties of a carbon-nanotube crystal, Phys. Rev. Lett. 73 (1994) 676–679.
[28] G. Chen, Y. Seki, H. Kimura, S. Sakurai, M. Yumura, K. Hata, D.N. Futaba, Diameter control of single-walled carbon nanotube forests from 1.3–3.0 nm by arc plasma deposition, Sci. Rep. 4 (2014).
[29] M.F. Yu, B.S. Files, S. Arepalli, R.S. Ruoff, Tensile loading of ropes of single wall carbon nanotubes and their mechanical properties, Phys. Rev. Lett. 84 (2000) 5552–5555.
[30] R.G. Ding, G.Q. Lu, Z.F. Yan, M.A. Wilson, Recent advances in the preparation and utilization of carbon nanotubes for hydrogen storage, J. Nanosci. Nanotechnol. 1 (2001) 7–29.
[31] Z.K. Tang, L.Y. Zhang, N. Wang, X.X. Zhang, G.H. Wen, G.D. Li, J.N. Wang, C. T. Chan, P. Sheng, Superconductivity in 4 angstrom single-walled carbon nanotubes, Science 292 (2001) 2462–2465.
[32] Q. Yu, W. Fu, C. Yu, H. Yang, R. Wei, M. Li, S. Liu, Y. Sui, Z. Liu, M. Yuan, G. Zou, G. Wang, C. Shao, Y. Liu, Fabrication and optical properties of large-scale ZnO nanotube bundles via a simple solution route, J. Phys. Chem. C 111 (2007) 17521–17526.
[33] J.Y. Moon, H. Kim, H.S. Lee, Synthesis and Formation Mechanism of ZnO Nanotubes via an Electrochemical Method, Korean, J. Met. Mater. 49 (2011) 400–405.
[34] J.Q. Hu, Q. Li, X.M. Meng, C.S. Lee, S.T. Lee, Thermal reduction route to the fabrication of coaxial Zn/ZnO nanocables and ZnO nanotubes, Chem. Mater. 15 (2003) 305–308.
[35] Y.J. Xing, Z.H. Xi, Z.Q. Xue, X.D. Zhang, J.H. Song, R.M. Wang, J. Xu, Y. Song, S. L. Zhang, D.P. Yu, Optical properties of the ZnO nanotubes synthesized via vapor phase growth, Appl. Phys. Lett. 83 (2003) 1689–1691.
[36] Y. Sun, G.M. Fuge, N.A. Fox, D.J. Riley, M.N.R. Ashfold, Synthesis of aligned arrays of ultrathin ZnO nanotubes on a Si wafer coated with a thin ZnO film, Adv. Mater. 17 (2005) 2477.
[37] T.M. Li, Z.A. Lin, L. Zhang, G. Chen, Controllable preferential-etching synthesis of ZnO nanotube arrays on SiO2 substrate for solid-phase microextraction, Analyst 135 (2010) 2694–2699.
[38] X.Y. Kong, Y. Ding, Z.L. Wang, Metal-semiconductor Zn-ZnO core-shell nanobelts and nanotubes, J. Phys. Chem. B 108 (2004) 570–574.
[39] G.S. Wu, T. Xie, X.Y. Yuan, Y. Li, L. Yang, Y.H. Xiao, L.D. Zhang, Controlled synthesis of ZnO nanowires or nanotubes via sol-gel template process, Solid State Commun. 134 (2005) 485–489.
[40] J.F. Yan, Y.M. Lu, H.W. Liang, Y.C. Liu, B.H. Li, X.W. Fan, J.M. Zhou, Growth and properties of ZnO nanotubes grown on Si(111) substrate by plasma-assisted molecular beam epitaxy, J. Cryst. Growth 280 (2005) 206–211.
[41] W.Z. Xu, Z.Z. Ye, D.W. Ma, H.M. Lu, L.P. Zhu, B.H. Zhao, X.D. Yang, Z.Y. Xu, Quasi-aligned ZnO nanotubes grown on Si substrates, Appl. Phys. Lett. 87 (2005).
[42] X. Shen, P.B. Allen, J.T. Muckerman, J.W. Davenport, J.-C. Zheng, Wire versus

tube: stability of small one-dimensional ZnO nanostructures, Nano Lett. 7 (2007) 2267–2271.
[43] Z. Zhou, Y. Li, L. Liu, Y. Chen, S.B. Zhang, Z. Chen, Size- and surface-dependent stability, electronic properties, and potential as chemical sensors: Computational studies on one-dimensional ZnO nanostructures, J. Phys. Chem. C 112 (2008) 13926–13931.
[44] C.S. Rout, S.H. Krishna, S.R.C. Vivekchand, A. Govindaraj, C.N.R. Rao, Hydrogen and ethanol sensors based on ZnO nanorods, nanowires and nanotubes, Chem. Phys. Lett. 418 (2006) 586–590.
[45] Z.C. Tu, X. Hu, Elasticity and piezoelectricity of zinc oxide crystals, single layers, and possible single-walled nanotubes, Phys. Rev. B 74 (2006).
[46] H. Xu, F. Zhan, A.L. Rosa, T. Frauenheim, R.Q. Zhang, First-principles study of the size-dependent structural and electronic properties of thick-walled ZnO nanotubes, Solid State Commun. 148 (2008) 534–537.
[47] A.D. Becke, Density-functional thermochemistry.3. the role of exact exchange, J. Chem. Phys. 98 (1993) 5648–5652.
[48] V.R.S.R. Dovesi, C. Roetti, R. Orlando, C.M. Zicovich-Wilson, F. Pascale, B. Civalleri, K. Doll, N.M. Harrison, I.J. Bush, P. D'Arco, M. Llunell, M. Causà, Y. Noël, CRYSTAL14 User's Manual, University of Torino, Torino, 2014.
[49] M.D. Towler, A. Zupan, M. Causa, Density functional theory in periodic systems using local Gaussian basis sets, Comput. Phys. Commun. 98 (1996) 181–205.
[50] S.H. Vosko, L. Wilk, M. Nusair, Accurate spin-dependent electron liquid correlation energies for local spin-density calculations-a critical analysis, Can. J. Phys. 58 (1980) 1200–1211.
[51] K.F. Moura, J. Maul, A.R. Albuquerque, G.P. Casali, E. Longo, D. Keyson, A. G. Souza, J.R. Sambrano, I.M.G. Santos, TiO2 synthesized by microwave assisted solvothermal method: Experimental and theoretical evaluation, J. Solid State Chem. 210 (2014) 171–177.
[52] C.W. Raubach, L. Polastro, M.M. Ferrer, A. Perrin, C. Perrin, A.R. Albuquerque, P. G.C. Buzolin, J.R. Sambrano, Y.B.V. de Santana, J.A. Varela, E. Longo, Influence of solvent on the morphology and photocatalytic properties of ZnS decorated CeO2 nanoparticles, J. Appl. Phys. 115 (2014).
[53] A.R. Albuquerque, J. Maul, E. Longo, I.M.G. dos Santos, J.R. Sambrano, Hydrostatic and 001 Uniaxial Pressure on Anatase TiO2 by Periodic B3LYP-D* Calculations, J. Phys. Chem. C 117 (2013) 7050–7061.
[54] J.P. Perdew, J.A. Chevary, S.H. Vosko, K.A. Jackson, M.R. Pederson, D.J. Singh, C. Fiolhais, Atoms, molecules, solids and surfaces: applications of the generalized approximation for exchange and correlation, Phys. Rev. B (1992) 6671.
[55] C. Adamo, V. Barone, Toward reliable density functional methods without adjustable parameters: the PBE0 model, J. Chem. Phys. (1999) 6158–6170.
[56] J.E. Moussa, P.A. Schultz, J.R. Chelikowsky, Analysis of the Heyd-Scuseria-Ernzerhof density functional parameter space, J. Chem. Phys. 136 (2012).
[57] J.E. Jaffe, A.C. Hess, Hartree-Fock study phase-changes in ZnO at high pressure, Phys. Rev. B 48 (1993) 7903–7909.
[58] T. Bredow, K. Jug, R.A. Evarestov, Electronic and magnetic structure of ScMnO3, Phys. Status Solidi B-Basic Solid State Phys. 243 (2006) R10–R12.
[59] D. R, C. M, O. R, R. C, S. VR, Ab-initio approach to molecular-crystals-a periodic Hartree-Fock study of crystalline urea, J. Chem. Phys. 12 (1990) 7402–7411.
[60] U. Ozgur, Y.I. Alivov, C. Liu, A. Teke, M.A. Reshchikov, S. Dogan, V. Avrutin, S. J. Cho, H. Morkoc, A comprehensive review of ZnO materials and devices, J. Appl. Phys. 98 (2005) 041301-1 041301-103.
[61] F. Decremps, F. Datchi, A.M. Saitta, A. Polian, S. Pascarelli, A. Di Cicco, J.P. Itie, F. Baudelet, Local structure of condensed zinc oxide, Phys. Rev. B 68 (2003) 1–10.
[62] N.L. Marana, V.M. Longo, E. Longo, J.B.L. Martins, J.R. Sambrano, Electronic and structural properties of the (10(1)over-bar0) and (11(2)over-bar0) ZnO surfaces, J. Phys. Chem. A 112 (2008) 8958–8963.
[63] R.C. Lima, L.R. Macario, J.W.M. Espinosa, V.M. Longo, R. Erlo, N.L. Marana, J. R. Sambrano, M.L. dos Santos, A.P. Moura, P.S. Pizani, J. Andres, E. Longo, J. A. Varela, Toward an understanding of intermediate- and short-range defects in ZnO single crystals. A combined experimental and theoretical study, J. Phys. Chem. A 112 (2008) 8970–8978.
[64] N.L. Marana, J.R. Sambrano, A.R. de Souza, Structural, electronic properties and elastic constants of ZnO, Quim. Nova 33 (2010) 810–815.
[65] R.W.G. Wyckoff, Crystal Structures, Interscience Publishers, New York, 1963.
[66] A. Ismach, L. Segev, E. Wachtel, E. Joselevich, Atomic-step-templated formation of single wall carbon nanotube patterns, Angew. Chemie-Int. Ed. 43 (2004) 6140–6143.
[67] V. Lacivita, A. Erba, Y. Noel, R. Orlando, P. D'Arco, R. Dovesi, Zinc oxide nanotubes: An ab initio investigation of their structural, vibrational, elastic, and dielectric properties, J. Chem. Phys. 214706 (138) (2013) 1–10.
[68] B. Wang, S. Nagase, J. Zhao, G. Wang, The stability and electronic structure of single-walled ZnO nanotubes by density functional theory, Nanotechnology 345706 (18) (2007) 1–6.
[69] F. Zhang, H. Cui, X. Ruan, W. Zhang, First-principles study of the (n, m) chiral ZnO nanotubes, J. Chem. Pharm. Res. (2014) 2069–2072.
[70] A.N. Imtani, V.K. Jindal, Structure of chiral single-walled carbon nanotubes under hydrostatic pressure, Comput. Mater. Sci. 46 (2009) 297–302.
[71] M.W. Zhao, Y.Y. Xia, Z.Y. Tan, X.D. Liu, F. Li, B.D. Huang, Y.J. Ji, L.M. Mei, Strain energy and thermal stability of single-walled aluminum nitride nanotubes from first-principles calculations, Chem. Phys. Lett. 389 (2004) 160–164.
[72] Z. Zhu, A. Chutia, R. Sahnoun, M. Koyama, H. Tsuboi, N. Hatakeyama, A. Endou, H. Takaba, M. Kubo, C.A. Del Carpio, A. Miyamoto, Theoretical study on electronic and electrical properties of nanostructural ZnO, Jpn. J. Appl. Phys. 47 (2008) 2999–3006.
[73] P. Russo, A. Hu, G. Compagnini, Synthesis, properties and potential applications of porous graphene: a review, Nano-Micro Lett. 5 (2013) 260–273.
[74] S. Reich, C. Thomsen, P. Ordejon, Electronic band structure of isolated and bundled carbon nanotubes, Phys. Rev. B 65 (155411) (2002) 1–11.